Construction and Building Materials 313 (2021) 125502

Contents lists available at ScienceDirect

Construction and Building Materials

journal homepage: www.elsevier.com/locate/conbuildmat

Carbonation curing for precast Engineered Cementitious Composites

Duo Zhang [a,b], Brian R. Ellis [a,b], Beata Jaworska [a,c], Wei-Hsiu Hu [a], Victor C. Li [a,b,*]

[a] Department of Civil and Environmental Engineering, University of Michigan, Ann Arbor, MI 48109, United States
[b] Center for Low-Carbon Built Environment, University of Michigan, Ann Arbor, MI 48109, United States
[c] Department of Building Materials Engineering, Institute of Building Engineering, Faculty of Civil Engineering, Warsaw University of Technology, Warsaw 00-637, Poland

ARTICLE INFO

Keywords:
Carbonation curing
Engineered Cementitious Composites
CO_2 sequestration
Permeability
Crack control

ABSTRACT

The ultra-durable Engineered Cementitious Composites (ECC) provides an opportunity for sequestering CO_2 during construction while reducing operational emissions in use phase. Here, ECC carbonation curing was investigated as a precast route of CO_2 sequestration. Results suggest that ECC sequesters 29.6% CO_2 by cement mass through early-age carbonation. The ultimate tensile and compressive strengths at 2 days were increased by 57.2% and 40.9%, respectively, while the tensile strain capacity attained 3.7%. Carbonation curing was found to densify the fiber/matrix interface resulting in higher interfacial bond, tighter crack widths, and more robust fiber bridging capacity. Consequently, the composite ultimate tensile strength increased by 22.7% while maintaining comparable strain capacity at 28 days. The tighter crack widths further decrease the material water permeability in loaded condition. These findings prove the feasibility of ECC carbonation curing and establish the scientific foundation of carbon utilization and permanent sequestration in ECC for precast construction elements.

1. Introduction

Carbonation curing is a recent technology for sequestering CO_2 in precast cementitious materials based on carbon mineralization [1]. At an early hydration age, unreacted calcium silicates and their early hydration products provide the Ca source to convert the dissolved CO_2 into $CaCO_3$. This process permanently locks up CO_2 and occurs at a faster rate than the normal cement hydration in a CO_2-free environment [2]. Consequently, the material early-strength development is accelerated, leading to a shorter turnaround time for curing of precast products and thus a higher precast manufacturing efficiency. In the long term, carbonating curing forms a hybrid microstructure comprised of hydration and carbonation products [3,4] which reportedly refines the material pore structure due to precipitation of $CaCO_3$ [5]. The reductions of pore size and pore volume improve the material resistance against air/liquid ingress [6,7] and potentially mitigate chloride-induced corrosion of the embedded reinforcing steel [8]. Apart from improvements in the pore structure and transport properties, carbonation curing is known to enhance concrete durability when exposed to sulfate [7,9,10], acid [7], and freeze–thaw environments [5]. Over the past decade, the concept of carbonation curing has been validated and demonstrated on a variety of precast products, such as dry-mix-based blocks [11], pipes [7], and the general wet-mix concrete [12].

Engineered Cementitious Composites (ECC) is a novel class of fiber-reinforced concrete with ultrahigh tensile ductility and intrinsically tight crack widths [13] independent of steel reinforcements. When loaded in tension, ECC has strain capacity at least two orders of magnitude that of conventional concrete and exhibits strain hardening and multiple fine cracking behaviors [14–16]. The design of ECC is guided by micromechanical principles, and the composite properties are governed by parameters associated with the cementitious matrix, fiber, and fiber/matrix interface [17,18]. Due to the microfiber bridging, the average crack width in ECC is generally below 100 μm and does not increase with the imposed strains [19]. The tight crack width lowers ECC's water permeability [20] and promotes self-healing [21–23], thus mitigating the operational carbon footprint by reducing the frequency of infrastructure repairs during the service life.

ECC's robust crack width control and low operational carbon can be synergized with the reduction of material embodied carbon through carbonation curing. To attain a desirable range of matrix toughness, coarse aggregate is eliminated from ECC compositions. This necessitates the use of high-volume cementitious ingredients providing additional opportunities for carbonation curing and enhancing CO_2 sequestration capacity. On the other hand, pore water in materials subjected to carbonation curing develop low pH, potentially limiting the applicability of steel rebar reinforcement due to the heightened concern of

* Corresponding author at: Department of Civil and Environmental Engineering, University of Michigan, Ann Arbor, MI 48109, United States.
E-mail address: vcli@umich.edu (V.C. Li).

https://doi.org/10.1016/j.conbuildmat.2021.125502
Received 16 August 2021; Received in revised form 23 October 2021; Accepted 30 October 2021
Available online 6 November 2021
0950-0618/© 2021 Elsevier Ltd. All rights reserved.

carbonation-induced corrosion. The high ductility and intrinsic crack control of ECC may lower the need for steel reinforcement and broaden the application of carbonation curing. In this manner, there is synergy between CO_2 sequestration in and structural durability of ECC structural elements.

To explore the opportunity offered by ECC for CO_2 sequestration, this study develops a carbonation curing process for precast ECC and examines its impact on the material properties. CO_2 uptake and mechanical properties are studied at both early age and standard 28 days, and the matrix and fiber/matrix interfacial properties are characterized under the micromechanics-based design framework. This study examines factors influencing the material transport properties to provide an estimate of durability; these factors include crack width, pore structure, and the coefficient of water permeability in crack/uncracked conditions. The experimental findings describe the feasibility of carbonation curing for precast ECC and to advance the opportunities of utilizing CO_2 in durable construction materials at scale.

2. Methodologies

2.1. Materials and mix proportions

Materials used for this study include ordinary Portland cement (PC, Type I, Lafarge-Holcim), fly ash (FA, Class F, Boral Resources), silica sand (F75, US Silica), high-range water reducer (HRWR, ADVA575, GCP Applied Technologies), and polyvinyl alcohol fiber (PVA, RECS15, Nycon). Tables 1-2 provide the PC and FA chemical compositions and the PVA fiber technical specification, respectively.

Two typical ECC compositions were studied, and the mix proportions are listed in Table 3. The mixtures chosen for this study have fly ash-to-cement (FA/PC) mass ratios of 1.2 and 2.2. These compositions have demonstrated high tensile ductility with tight cracks [21,24]. Both mixtures were studied for CO_2 uptake and changes to mechanical properties, while only one of them was selected for characterization of microstructure and transport properties. The workability of the fresh ECC was evaluated by the flow table test (cf. ASTM C230) and was controlled within 220 ± 10 mm.

2.2. Mixing and casting

A 12 L capacity Hobart mixer was used for mixing. The mixing procedure is elaborated as follows:

- Step 1: dry-mix PC, FA and silica sand at a low speed for 1 min
- Step 2: mix water and HRWR, then add to the solid ingredients
- Step 3: mix the mortar at a low speed for 3 min; pause and scrap the bowl sides to transfer the collected mortar into the batch; mix at medium speed for 1 min
- Step 4: add PVA fiber; mix at medium speed for 3 min

The fresh ECC was cast into dogbone-shaped specimens for uniaxial tension (see Fig. 1) and 50-mm cubes for unconfined compression. All specimens were stored in open air after casting and demolded after 24 h. The demolded specimens were then separated into two groups for carbonation curing and normal hydration (i.e., non-carbonated reference), respectively. The non-carbonated group was designed as a control and cured under room conditions (23 ± 2 °C, RH 60 ± 5%) until the defined testing ages.

Table 1
PC and FA compositions (by mass %).

Composition	PC	Fly ash
CaO	67.5	3.4
SiO_2	17.7	52.2
Al_2O_3	4.2	22.2
MgO	2.0	0.9
P_2O_5	0.1	0.1
Fe_2O_3	3.7	13.5
K_2O	0.5	2.6
TiO_2	0.3	1.0
SO_3	3.6	2.2
LOI	2.1	1.0

Table 2
PVA fiber technical specification.

Length (mm)	Diameter (μm)	Elongation (%)	Density (kg/m^3)	Young's modulus (GPa)	Tensile strength (MPa)
8	39	6	1300	42.8	1600

Table 3
ECC mix proportions.

Mixing compositions	Mix I (FA/PC = 1.2)	Mix II (FA/PC = 2.2)
Portland cement (PC)	1	1
Fly ash (FA)	1.2	2.2
Silica sand	0.8	0.79
Water	0.58	1.16
HRWR	0.007	0.013
PVA fiber, vol%	2	2

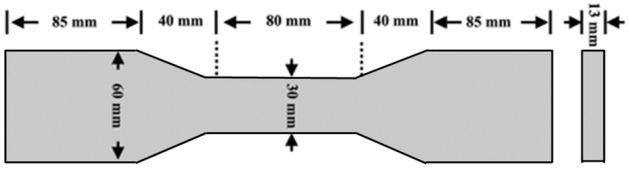

Fig. 1. Dimensions of dogbone-shaped specimen for uniaxial tension.

2.3. Curing regime

The execution of ECC carbonation curing followed the typical procedure of conventional concrete [12] and was adapted to a longer preconditioning treatment due to the delayed setting time associated with the high-volume FA incorporation. A four-step process was conducted including 1) in-molding curing, 2) off-mold conditioning, 3) carbonation, and 4) subsequent curing. Fig. 2 depicts the timing, processing, and exposure conditions at each step. Fresh ECC was first set in steel molds (dogbone/cube) until hardened at 18 h under room conditions. The specimens were then demolded and subjected to an enforced drying process (i.e., de-mold conditioning). This process aims to partially remove the pore water to evacuate adequate porous paths to facilitate CO_2 diffusion. Previous studies [25,26] suggest that 40% water removal provides the maximal efficiency of CO_2 uptake and was thus chosen as the target for ECC. In the laboratory condition (23 ± 2 °C, RH 60 ± 5%), it took approximately 6 h to complete the drying process. After the off-mold conditioning, the partially dried specimens were mounted into a bench-top pressure chamber (see Fig. 3) for carbonation. The chamber was filled and supplied continuously with high-purity CO_2 gas (99.8% concentration) at 5 bar (0.5 MPa) at room temperature (23 ± 2 °C). Carbonation was conducted for up to 24 h, such that the early-age curing process (Steps 1-3) was completed within 48 h.

After carbonation, a group of specimens was tested immediately (i.e., at 48 h or 2 days) for carbonation depth, CO_2 uptake, and mechanical properties, while the other group was stored in air until the standard 28 days. The non-carbonated control was tested at 2 and 28 days following the same testing protocol as for the carbonated groups.

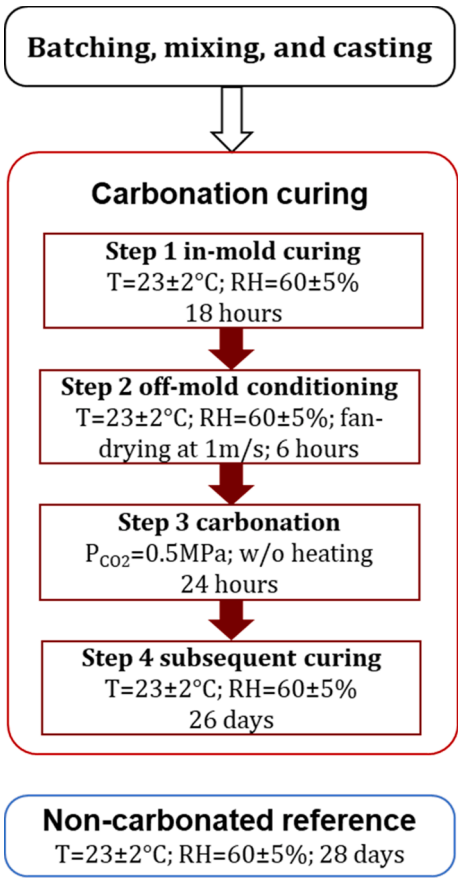

Fig. 2. Curing procedure. For the carbonated specimens, Steps 1–3 comprise the 48-hour carbonation curing process.

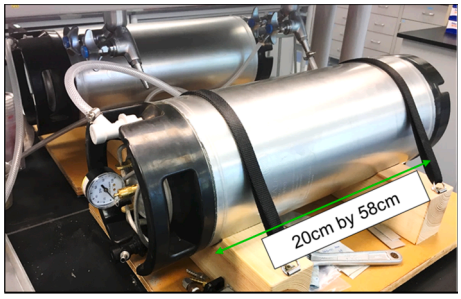

Fig. 3. Lab-scale pressure chamber for carbonation curing.

2.4. Material characterization

2.4.1. CO_2 uptake estimate

Carbonation curing is a mass gain process due to the precipitation of mineral carbonates from gaseous CO_2, which is an energetically favorable exothermic reaction. The heat of reaction drives the free water to evaporate from samples and subsequently condense inside the chamber. In general, CO_2 uptake in this process can be estimated via two approaches. One is based on the system mass balance, known as the mass gain method [12,26,27], while the other is based on thermal analysis of the carbonated sample, such as through thermogravimetric analysis (TGA) [2,28]. The two approaches were adopted independently for estimating CO_2 uptake in ECC and the average was reported.

For the mass gain method, CO_2 uptake is determined following Eq. (1). Note that the water condensed inside the chamber originated in ECC's mixing water, thus should be added to the specimen mass after carbonation. Upon the completion of carbonation, the condensed water was collected using an absorbent paper [29] and weighed at an accuracy of 0.01 g.

$$\mathrm{CO_2uptake}(\%) = \frac{m_2 + m_{\mathrm{water}} - m_1}{m_{\mathrm{cement}}} \times 100\% \tag{1}$$

where

m_1 and m_2 are the sample masses weighed before and after carbonation, respectively
m_{water} is the mass of the condensed water
m_{cement} is the dry cement mass in the sample

CO_2 uptake can also be measured from the sample mass loss during the decarbonation stage upon heating. Due to the incorporation of silica sand and fibers in ECC, a muffle furnace was used instead of TGA. As TGA requires a small quantity of powder samples, the sampling process (e.g., grinding and sieving) involves the experimental variability associated with the sand and fiber contents among different TGA samples. The muffle furnace method can handle larger samples without grinding or sieving and thus can avoid this variability. The dogbone-shaped specimens were sliced along the cross section into 5-mm thick pieces. About 100 g of the sliced sample was heated in a muffle furnace from room temperature to 550 °C and 950 °C. The mass change between 550 °C and 950 °C is assumed to be the mass of CO_2 released from the sample. The CO_2 uptake can be determined following Eq. (2).

$$\mathrm{CO_2\ uptake}(\%) = \frac{(m_{550} - m_{950}) - (M_{550} - M_{950})}{m_{\mathrm{cement}}} \times 100\% \tag{2}$$

where

m_{950} and m_{550} are the masses of carbonated sample at 950 °C and 550 °C, respectively
M_{950} and M_{550} are the masses of non-carbonated reference at 950 °C and 550 °C, respectively
m_{cement} is the dry cement mass in the sample

2.4.2. Mechanical testing

The mechanical testing includes unconfined compression and uniaxial tension at 2 and 28 days. The compression test was conducted on the 50-mm ECC cubes using a Forney loading machine at a loading rate of 0.5 MPa/s (cf. ASTM C109). The uniaxial tension test was conducted on the dogbone-shaped specimens with a gauge length of 80 mm (cf. JSCE [30]). Two linear variable displacement transducers (LVDT) were mounted to the specimen to record the gauge length elongation every second. The loading process was displacement-controlled using an Instron loading system at a constant rate of 0.5 mm/min. Each mechanical test included four repetitions and the average was reported.

ECC matrix toughness K_m was determined experimentally as per ASTM E399. The test was conducted on a pre-notched matrix specimen (without fiber) subjected to three-point bending. The beam specimen measured 304.8 mm in length by 76.2 mm in height by 38.1 mm in depth. The loading support spanned 254 mm. The notch-to-height ratio was 0.4. Due to the nature of CO_2 diffusion, carbonation occurs to the highest extent on surface and the lowest in core. To ensure the material adjacent to the notch tip was carbonated effectively, matrix specimens were pre-notched before carbonation. The loading process was displacement-controlled at a rate of 0.5 mm/min. K_m is calculated using:

$$K_m = \frac{PS}{bw^{3/2}} \cdot f\left(\frac{a}{w}\right) \tag{3}$$

$$f\left(\frac{a}{w}\right) = 3\sqrt{\frac{a}{w}} \cdot \frac{1.99 - \left(\frac{a}{w}\right)\left(1 - \frac{a}{w}\right)\left[2.15 - 3.93\frac{a}{w} + 2.7\left(\frac{a}{w}\right)^2\right]}{2\left(1 + 2\frac{a}{w}\right)\left(1 - \frac{a}{w}\right)^{3/2}} \tag{4}$$

where

K_m is fracture toughness in MPa $\sqrt{m}$
P is the peak load in N
S is the span in m
b is the specimen thickness in m
w is specimen width in m
a is the notch depth in m

2.4.3. Crack width measurement

ECC's crack width was measured on the dogbone-shaped specimens while loaded in tension. The laboratory setup documented by Liu et al. [12] was adopted to load the specimen to a selected tensile strain and subsequently lock the specimen in tension by a pair of bolts and nuts. The surface of the loaded specimen was then examined for crack width distribution along the centerline using a bench-top optical microscope at 50× magnification. Unlike conventional concrete, the micro-cracks in ECC continue carrying load due to the fiber bridging and may be subjected to partial closure when the load is released. A prior study by Yang et al. [31] suggested that the loaded crack width could double the residual crack width measured on the same specimen after unloading. Hence, measuring the loaded cracks is necessary to emulate the field condition.

2.4.4. Selective acid dissolution

Early-age carbonation is known to compromise the binder alkalinity and thus may hinder pozzolanic reactions at later ages [26]. To clarify this effect in ECC, the reaction degree of fly ash was determined experimentally using the selective dissolution method recommended by RILEM TC238 [32]. The selective dissolution method assumes that Portland cement and reacted fly ash dissolve in acid, leaving the unreacted fly ash the only phase in the residue. This is not valid ideally due to the undesired dissolution of a minor part of the unreacted fly ash and other phases that may be undissolved. The testing accuracy can be improved by applying calibration of the raw materials and residues [32], and the results are more reliable in the presence of higher volumes of fly ash. As the ECC mixtures used in this study had a minimum fly ash-to-cement ratio of 1.2, the selective dissolution method could be adopted for its high consistency. The test was conducted on powdered samples (passing 75 μm sieve) uniformly collected from the carbonation-cured and non-carbonated ECC cement pastes at 28 days. Salicylic acid and hydrochloride acid were used for preparing the acid solution, and the proportion is given in [32].

2.4.5. Mercury intrusion porosimetry (MIP)

The pore structure was analyzed on ECC samples using MIP. After stopping the hydration of sliced ECC samples through solvent exchange (isopropanol) at 28 days, the samples were vacuum-dried in a desiccator with silica gel. The MIP test was conducted using a Micromeritics AutoPore Porosimeter. The contact angle of mercury was set as 130°, and the intrusion pressure was up to 420 MPa corresponding to a minimum pore diameter of 3 nm.

2.4.6. Single fiber pullout test

To characterize the fiber/matrix interfacial bond, the single fiber pullout test was performed using a 5 N load cell at a constant loading rate of 0.5 mm/min. The test followed the same configuration as reported by Redon et al. [33], and the load–displacement (P-S) curves were collected. Fig. 4 illustrates a typical P-S curve, where the PVA fiber experiences a debonding stage and a subsequent slippage stage. During the debonding stage, the PVA fiber pullout load P increases up to P_a followed by a sudden drop to P_b as the fiber is completely debonded from the matrix. The surface abrasion of the ductile PVA fiber accounts for the slip hardening phenomenon during the slippage stage, where the pullout load continues increasing as a function of the fiber displacement.

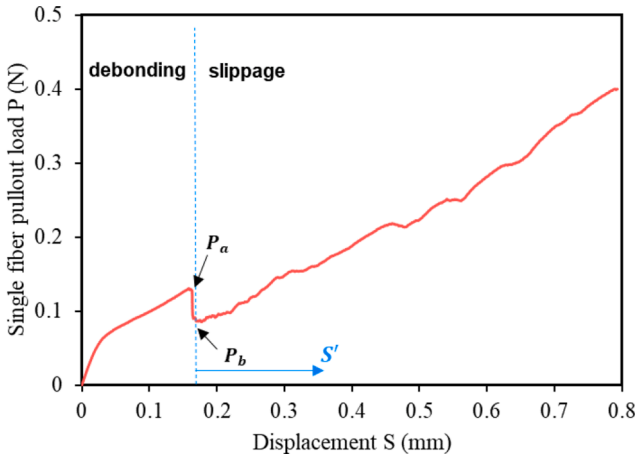

Fig. 4. Typical single-fiber pullout P-S curve.

The fiber/matrix interfacial bond properties, including chemical debonding energy G_d (i.e., chemical bond in J/m^2), frictional bond τ_0 (in MPa), and slip-hardening coefficient β can be determined as follows [33]

$$G_d = \frac{2(P_a - P_b)^2}{\pi^2 E_f d_f^3} \tag{5}$$

$$\tau_0 = \frac{P_b}{\pi d_f l_e} \tag{6}$$

$$\beta = \frac{d_f}{l_e}\left(\frac{1}{\pi \tau_0 d_f} \cdot \frac{\Delta P}{\Delta S'}\bigg|_{s' \to 0} + 1\right) \tag{7}$$

where

E_f is the Young's modulus of PVA fiber
d_f is the fiber diameter
l_e is the fiber embedded length
$\Delta P/\Delta S'$ is the initial slope of the P-S load defined in Fig. 4

2.4.7. Backscattered electron microscopy (BSE)

To understand plausible alterations at the fiber/matrix interface, the matrix close to the fiber surface was examined via backscattered electron microscopy (BSE) on a scanning electron microscope (SEM). Polished ECC samples were observed at a 1000× magnification using a JEOL IT-500 SEM equipped with energy dispersive spectroscopy (EDS). The observation was conducted at a 20 kV acceleration voltage and a 40 mA current.

2.4.8. Micromechanical modeling

The purpose of modeling efforts is to determine the fiber bridging capacity σ_0 and complementary energy J_b' and to assess the effect of carbonation curing on the strain-hardening potential based on ECC's micromechanical design framework [13]. Experimental data obtained from the tests above were used as input. The calculation follows the fiber bridging constitutive law that links the single fiber/matrix interaction at microscale to the single crack fiber bridging behavior at mesoscale [34]. Based on the results, pseudo strain-hardening (PSH) indices can be determined

$$\mathrm{PSH}_{\mathrm{energy}} = \frac{J_b'}{J_{tip}} \tag{8}$$

$$\mathrm{PSH}_{\mathrm{strength}} = \frac{\sigma_0}{\sigma_c} \tag{9}$$

$$J_{tip} = \frac{K_m^2}{E_m} \quad (10)$$

where

E_m is the Young's modulus of matrix in GPa
K_m is the matrix toughness in MPa $\sqrt{m}$

2.4.9. Water permeability

The water permeability test was conducted on the non-cracked dogbone-shaped specimens and on the cracked specimens pre-strained to 1%, 2% and 3% in tension. A falling head test setup developed in prior studies [12,20] was used to measure the coefficient of permeability. The test began at the age of 28 days. All specimens were sealed with epoxy on the sides and were saturated for 48 h before testing. The water permeability setup is shown schematically in Fig. 5. The coefficient of permeability k is calculated as follows

$$k = \frac{a \bullet L}{A \bullet t_f}\left(\frac{h_0}{h_f}\right) \quad (11)$$

where

k is the coefficient of permeability (m/s)
a is the cross-sectional area of the standpipe (m), i.e., 2.84×10^{-5} m^2
L is the specimen thickness in the flow direction, i.e., 0.012 m
A is the top surface area of the specimen subject to the flow, i.e., 8.93×10^{-3} m^2
t_f is the elapsed time (s)
h_0 and h_f are the initial and final water heads (m), respectively.

3. Results and discussion

3.1. Carbonation behavior and pozzolanic reaction

ECC appears to be highly reactive to CO_2 at the early age. Fig. 6 shows the evolution of CO_2 uptake in the dogbone-shaped ECC specimens after various carbonation durations. The average CO_2 uptake in Mix I was found to attain 21.0% within only 1 h and up to 29.6% after 24 h. Mix II with a higher fly ash content exhibited a faster reaction process and achieved 35.1% CO_2 uptake at 24 h. Compared to the carbonation behavior of conventional mortar and concrete [3,26,35], ECC exhibits a remarkable CO_2 reactivity in early carbonation. This can be attributed to the high-volume fly ash incorporation [26], which dilutes cement particles and increases the contact between dissolved CO_2 and Ca-bearing phases. A similar effect was observed in [26] where the

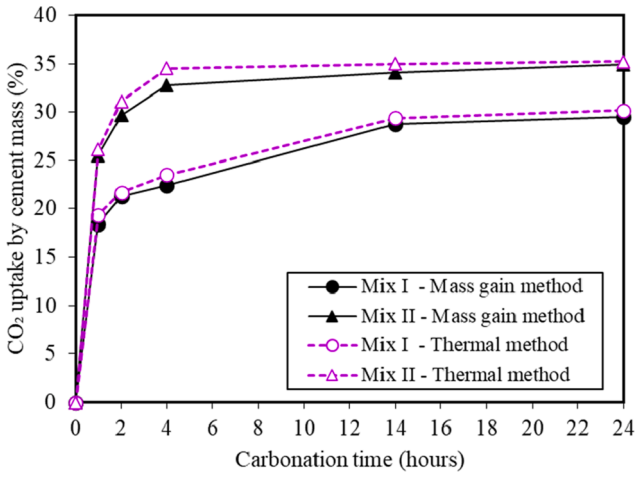

Fig. 6. Evolution of estimated CO_2 uptake in dogbone-shaped ECC specimens.

24-hour CO_2 uptake increased from 19.57% to 28.20% with reference to the mass of cement when incorporated with 50% fly ash.

The depth of carbonation was measured on saw-cut cross sections of ECC specimens by spraying the sample with phenolphthalein indicator. After 24 h of carbonation, the dogbone-shaped specimen was found to be fully carbonated, whereas cube specimens exhibited a layered structure comprised of a carbonated surface (11–15 mm) and a non-carbonated core. Fig. 7 compares the CO_2 uptake and carbonation depth of different ECC specimens. The inhomogeneous carbonation along the depth accounts for the lower average CO_2 uptake observed for cubes compared to the thin dogbone-shaped specimens. Relative to Mix I, the Mix II cube specimens containing more fly ash showed a higher CO_2 uptake and a larger depth of carbonation.

XRD was conducted at 28 days to verify the mineralogical alterations associated with carbonation curing. As indicated in Fig. 8, the main mineral form of carbonation products was found to be calcite. Due to the intense carbonation of ECC, portlandite and ettringite were mostly depleted, leaving calcite the most prominent crystalline phase in the binder. This is consistent with the findings of previous studies [3,35] and indicates that carbonation curing forms a low-alkalinity environment which may limit its applicability to steel-reinforced structural elements.

The pozzolanic reaction of fly ash in ECC was substantially lowered after carbonation curing. As shown in Fig. 9, the early carbonation nearly depleted the pozzolanic reaction at 28 days, resulting in a decrease of the reacted fly ash fraction from 11.2% to 0.2% for Mix I and from 6.4% to 0% for Mix II. The calcium hydroxide reduction at the early

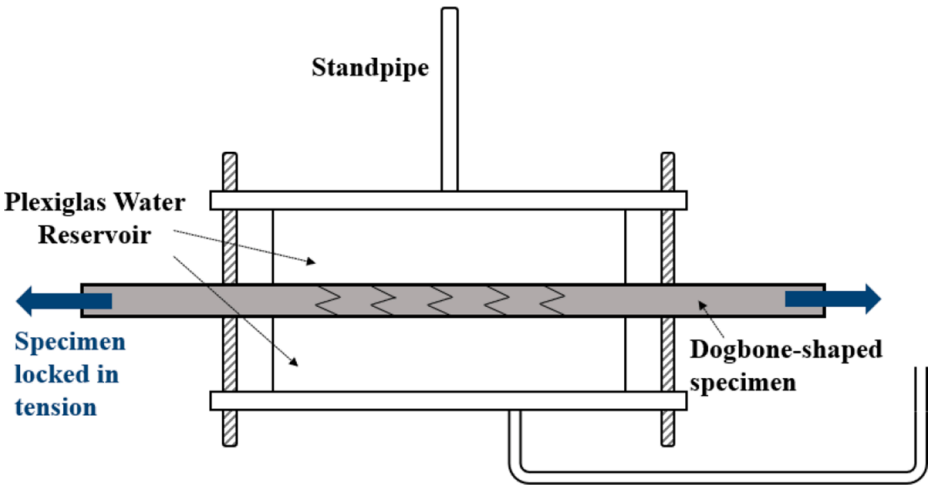

Fig. 5. Falling head permeability test setup schematic.

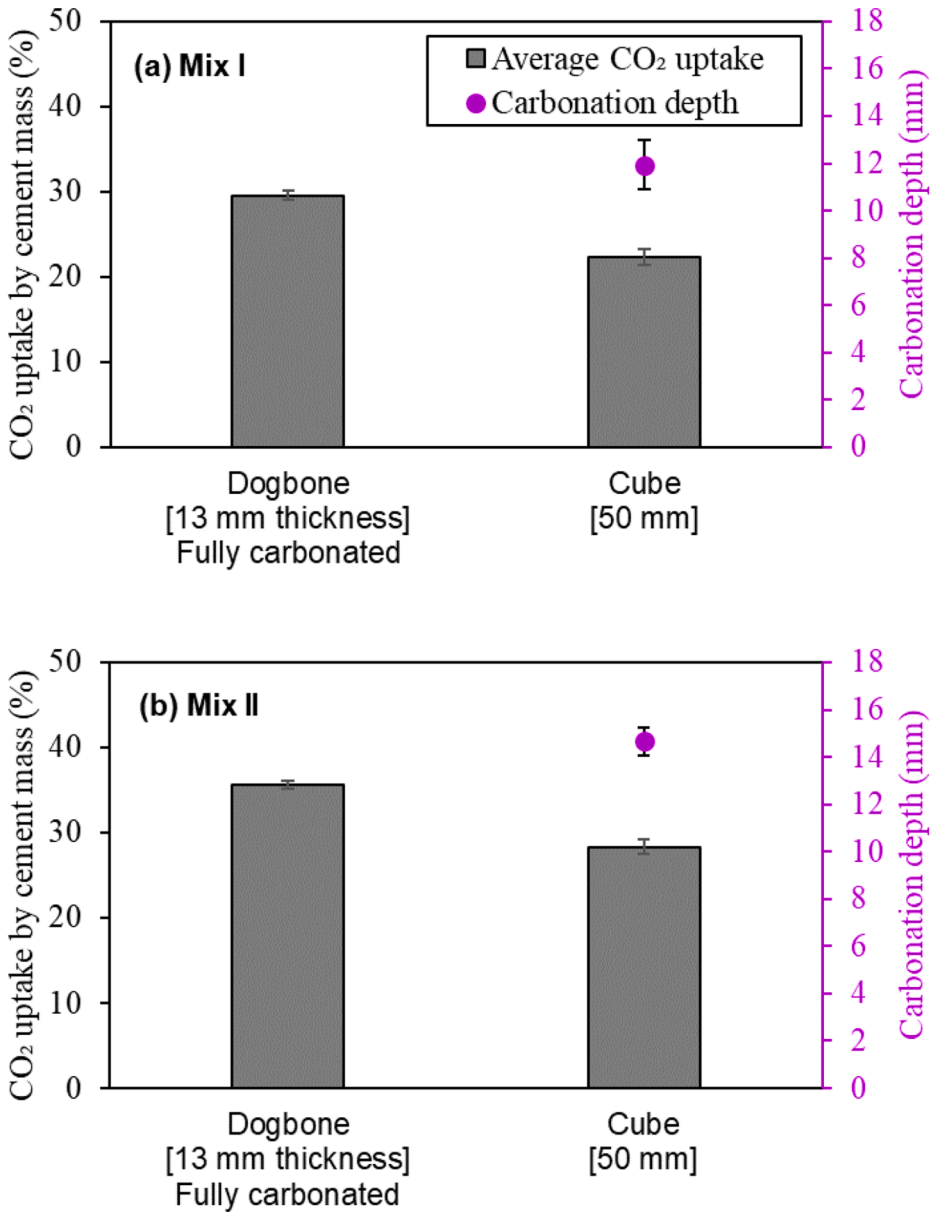

Fig. 7. Average CO_2 uptake and carbonation depth in ECC subject to 24-hour carbonation.

age accounted for the loss of fly ash reaction [26]. As the matrix was severely carbonated with an average CO_2 uptake up to 35.1% by cement mass, the subsequent cement hydration was not capable of recovering the calcium hydroxide level for pozzolanic reaction. It indicates that most fly ash in the carbonated ECC acts as fillers or micro-aggregates and does not participate in the pozzolanic process.

3.2. ECC mechanical properties

Carbonation curing accelerates early strength gain for both ECC mixtures but leads to different mechanical properties at 28 days for Mixes I and II. As shown in Fig. 10, at 2 days, carbonation curing increased ECC's compressive strength from 27.6 MPa to 38.9 MPa (by 40.9%) for Mix I and from 20.1 MPa to 29.5 MPa (by 46.8%) for Mix II. The noticeably high early strength induced by carbonation curing is evident for the effective CO_2 uptake in ECC. After the early carbonation, the compressive strength of Mix I continued increasing and reached 54.0 MPa after a 26-day subsequent air curing, which was comparable to the non-carbonated reference recording 52.6 MPa. In comparison, for Mix II at the same age, carbonation curing was found to lower the compressive strength by 15.5% (from 42.7 MPa to 36.1 MPa at 28 days). It appears that the post-carbonation strength development was slowed down in Mix II containing a higher fly ash content. This phenomenon could be attributed to the loss of pozzolanic reaction in the carbonated specimens and is suggestive of a trade-off relation between the early carbonation and fly ash pozzolanic reaction, due to their intrinsic competition for calcium hydroxide [26]. As the cement content decreases and fly ash increases, the strength enhancement by carbonation does not compensate for the strength loss associated with the reduced pozzolanic reaction. Nevertheless, it seems that Mix I with a 1.2 FA/PC ratio is desirable to attain a high early strength (and CO_2 uptake) while maintaining a comparable long-term strength.

The typical tensile stress–strain curves are shown in Fig. 11, and the tensile properties are summarized in Table 4. At 2 days, carbonation curing increased the first-cracking strength, ultimate tensile strength, and strain capacity for both mixtures. The carbonation-cured Mix I ECC attained the highest ultimate tensile strength recording 4.59 MPa at 2 days, exceeding its non-carbonated counterpart by 57.2%. At 28 days,

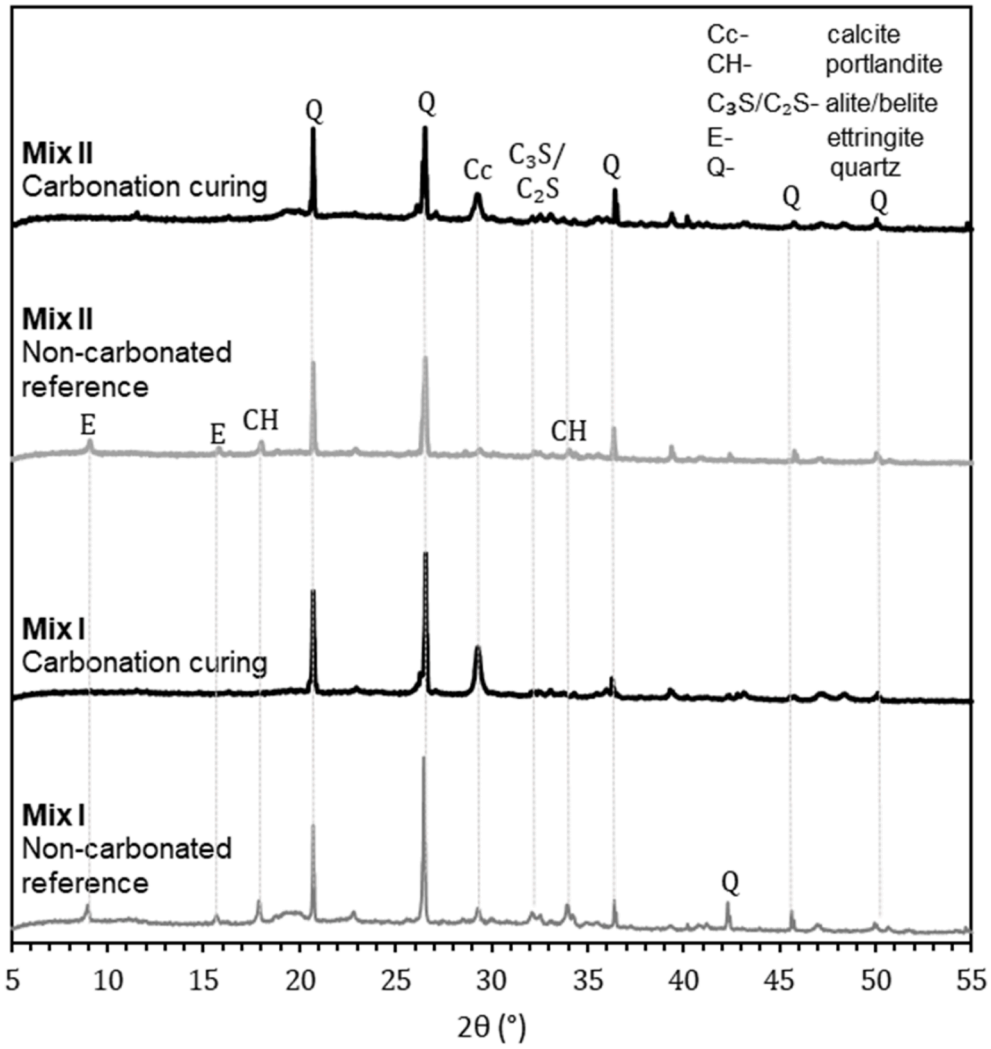

Fig. 8. XRD patterns of ECC at 28 days.

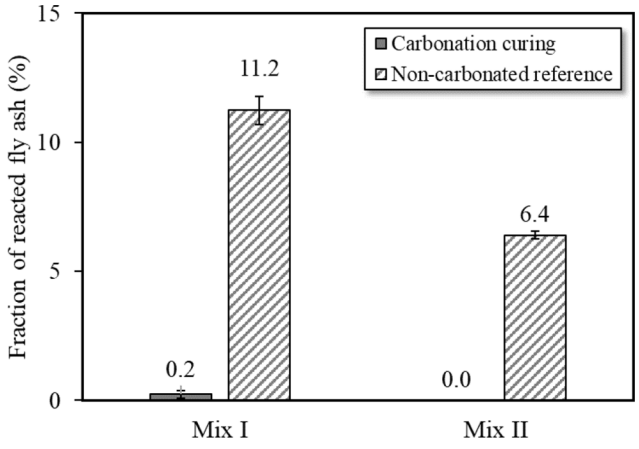

Fig. 9. Fly ash reaction degree in ECC at 28 days.

carbonation curing maintained higher ECC tensile strengths and a comparable strain capacity for Mix I but appeared to compromise both strength and ductility for Mix II. As noted in Table 4, the ultimate tensile strength of Mix I at 28 days was improved by carbonation curing from 6.47 MPa to 7.94 MPa, while attaining a tensile strain capacity of 4.42%. Nevertheless, for Mix II subjected to carbonation curing, the first-cracking and ultimate tensile strengths at 28 days were found to decrease by 18.2% and 29.8% respectively, and the strain capacity was lowered from 3.64% to 2.88%. The results of uniaxial tension tests confirm the positive impact of carbonation curing on Mix I that results in higher tensile strength at both early age and 28 days. At FA/PC ratios over 2.2, however, carbonation curing decreases ECC's long-term strength and may raise the uncertainty of net carbon benefits when normalized to material properties [36]. Therefore, Mix I is recommended for carbonation curing and was chosen for further characterization in the following sections.

3.3. Micromechanical analyses

The effect of carbonation curing on ECC's micromechanical parameters was analyzed on the fiber-free matrix and on the composite at two length scales. At microscale, the fiber/matrix interfacial bond was characterized through the single-fiber pullout test [33] and examined through combined BSE/EDS analysis. At mesoscale, the fiber bridging capacity σ_0 and strain hardening potential were estimated based on the micromechanical modeling.

3.3.1. Matrix property

The modulus of elasticity E_m and fracture toughness K_m represent the key factors related to matrix. At 28 days, carbonation curing was found to increase E_m and marginally affect K_m. As shown in Table 5, E_m was

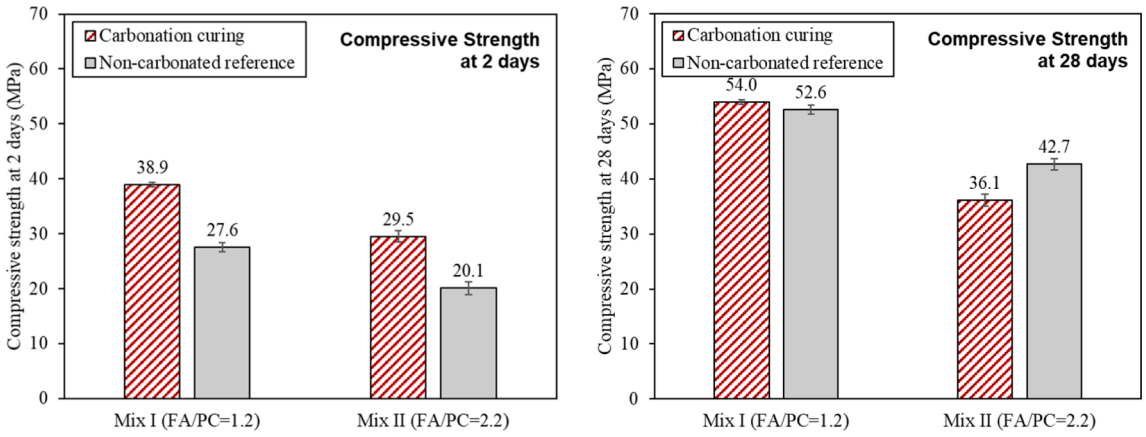

Fig. 10. ECC compressive strength.

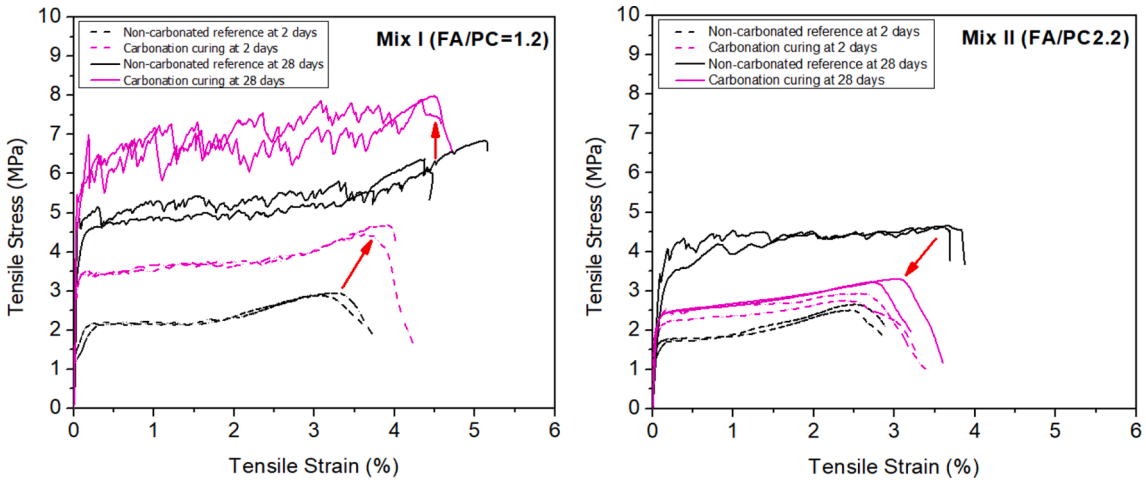

Fig. 11. Tensile strength/ductility enhanced for Mix I but reduced for Mix II by carbonation curing.

Table 4
Tensile properties of ECC mixtures.

Specimen group	Testing age, day	First-cracking strength, MPa	Ultimate tensile strength, MPa	Tensile strain capacity, %
Mix I-carbonation curing	2	3.37 ± 0.21	4.59 ± 0.15	3.72 ± 0.30
	28	5.30 ± 0.37	7.94 ± 0.07	4.42 ± 0.11
Mix I- non-carbonated reference	2	1.24 ± 0.06	2.92 ± 0.04	3.11 ± 0.08
	28	4.21 ± 0.03	6.47 ± 0.53	4.77 ± 0.50
Mix II-carbonation curing	2	1.69 ± 0.18	2.84 ± 0.13	2.51 ± 0.14
	28	2.48 ± 0.11	3.27 ± 0.06	2.88 ± 0.23
Mix II- non-carbonated reference	2	1.06 ± 0.06	2.59 ± 0.11	2.49 ± 0.08
	28	3.40 ± 0.25	4.66 ± 0.02	3.64 ± 0.04

Table 5
Matrix properties for Mix I at 28 days.

Curing condition	E_m (GPa)	K_m (MPa·m$^{1/2}$)
Carbonation curing	24.2 ± 2.0	0.415 ± 0.021
Non-carbonated reference	21.5 ± 1.1	0.426 ± 0.025

measured 24.2 GPa after carbonation curing and 21.5 GPa for the non-carbonated reference, indicating a 12.6% increase ensuing from carbonation. The carbonation-induced increase of E_m was reported previously in traditional concrete [37] and could be attributed to the total porosity reduction due to $CaCO_3$ precipitation. By contrast, K_m was found to be 0.415 MPa·m$^{1/2}$ and 0.426 MPa·m$^{1/2}$ with and without carbonation curing, respectively. The marginal reduction in K_m indicates that the matrix may become slightly more brittle after carbonation curing. This impact seemed to be trivial compared to the experimental variability.

3.3.2. *Microscale: fiber/matrix interface*

At the microscale, carbonation curing was found to enhance the fiber/matrix interfacial bond by depositing $CaCO_3$ along the fiber/matrix interface. Table 6 illustrates the alterations of chemical bond G_d and frictional bond τ_0 obtained from the single fiber pullout test at 28 days. Carbonation curing increased G_d from 0.26 J/m^2 to 1.67 J/m^2 and τ_0 from 1.70 MPa to 2.11 MPa, indicating a stronger resistance to fiber debonding and slippage. This phenomenon is evidenced from the BSE observation shown in Fig. 12a, where solid precipitates were observed at

Table 6
Fiber/matrix interfacial bond for Mix I at 28 days.

Curing condition	G_d (J/m^2)	τ_0 (MPa)	β
Carbonation curing	1.67 ± 1.41	2.11 ± 1.01	0.56 ± 0.32
Non-carbonated reference	0.26 ± 0.23	1.70 ± 0.84	0.58 ± 0.16

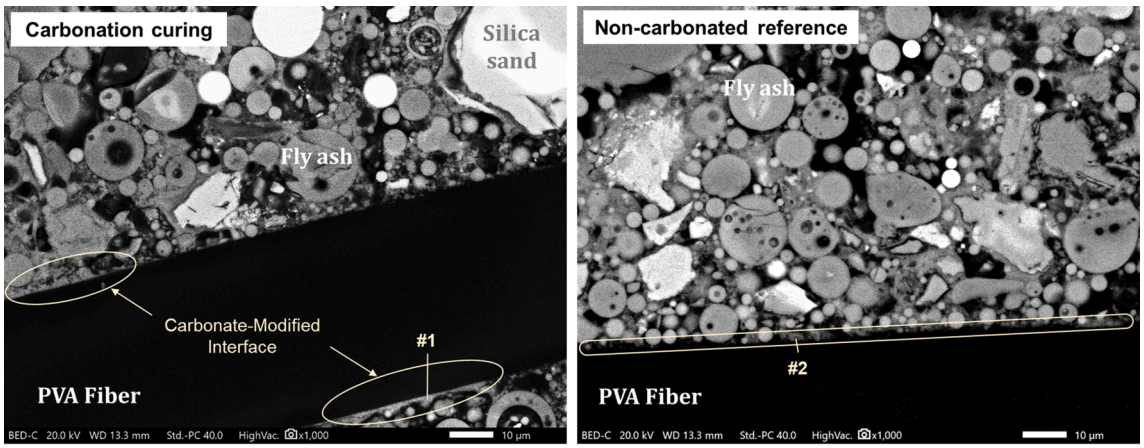

(a) BSE images (magnification at ×1000)

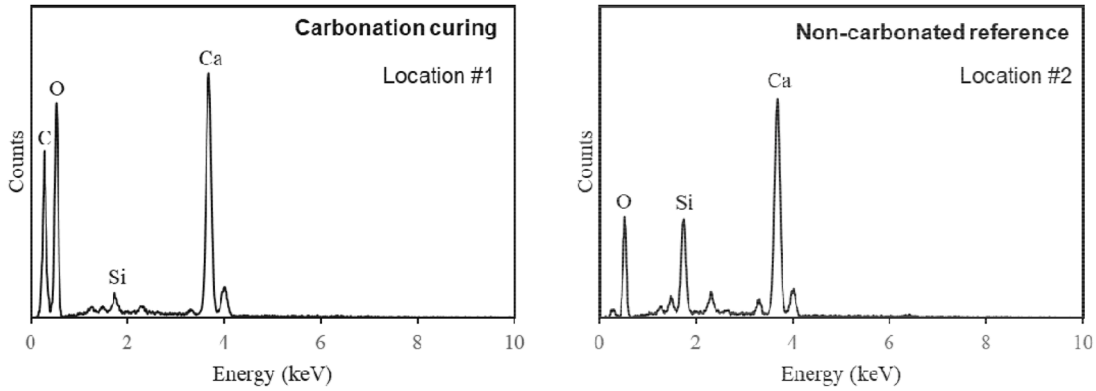

(b) EDS point spectrums at fiber/matrix interface

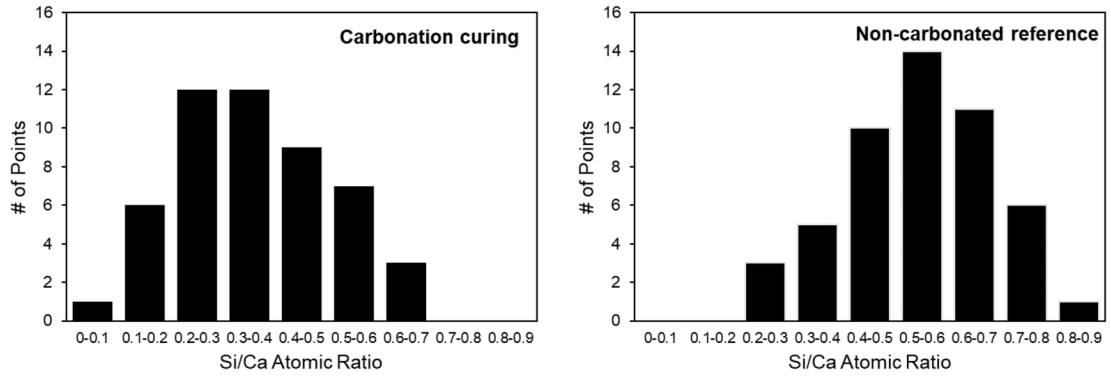

(c) Histogram of Si/Ca atomic ratio at fiber/matrix interface

Fig. 12. SEM-BSE/EDS characterization of fiber/matrix interface for Mix I at 28 days.

several interfacial sites, seemingly acting as a 'coating' along the fiber surface in the carbonated sample. The EDS analysis in Fig. 12b-c indicates strong elemental signals of Ca and C with a small intensity of Si, suggesting the primary precipitate is $CaCO_3$, whereas the non-carbonated reference shows the co-existence of Ca and Si in the absence of C. It can be inferred that the $CaCO_3$ precipitated from early carbonation accounts for the stiffened matrix close to PVA fibers and thus increases the fiber/matrix interfacial frictional bond. This effect appears to be localized and discontinuous along the fiber length. The increase of chemical bond, however, is associated with potential alterations of Ca^{2+} and Al^{3+} bearing phases [24], and their interactions with the PVA fiber warrant further investigation.

The slip hardening coefficient β was measured as 0.56 and 0.58 for the carbonated and non-carbonated samples, respectively. The slip hardening phenomenon is commonly associated with the surface abrasion of polymeric fibers during the pullout process. In the 'tunnel' space formed between fiber and matrix, the accumulated fiber debris induces a 'jamming' effect that requires a higher load to further pullout the fiber [13]. The slip hardening process seems to not be substantially influenced by carbonation curing.

3.3.3. Mesoscale: fiber bridging capacity and strain-hardening indices

The mesoscale analysis validates the strain-hardening performance of ECC but indicates a reduction of the strain-hardening potential after carbonation curing. Based on the ECC micromechanics model [13], the fiber bridging behavior is determined using experimental inputs of fiber/matrix interfacial bond and matrix properties. The calculated fiber bridging curves are shown in Fig. 13, and the corresponding PSH indices are listed in Table 7. All PSH indices were above the value of unity, suggesting that the strain hardening criteria could be achieved for both carbonation curing and non-carbonated reference. Nevertheless, carbonation curing was found to decrease PSH_{energy} from 33.2 to 29.2 and $PSH_{strength}$ from 2.00 to 1.62, resulting in smaller margins with respect to 1. This is suggestive of a decreased strain-hardening potential due to carbonation curing, which lowers the material's capability to accommodate possible inhomogeneity and variation. In these cases, the composite performance could be restored under the guidance of ECC's design framework [13].

3.4. Transport properties

Transport properties are important for understanding the durability of cementitious materials. In field structures, the ingress of air and liquid occurs through the interconnected porous space in non-cracked materials and through both cracks and pores in cracked materials. Hence, the effect of carbonation curing was first investigated on ECC's pore structure and micro-cracks and was then validated by the coefficient of water permeability measured on loaded ECC specimens.

Fig. 14 and Tables 8-9 show the pore size distribution and key indicators of the composite pore structure at 28 days. It was found that carbonation curing lowered the total porosity but tended to increase the pore size. As shown in Table 8, the total porosity decreased from 20.2% to 18.5% after carbonation curing, whereas the median diameter increased from 152 nm to 224 nm. On the differential pore size distribution curve depicted in Fig. 14b, the peak location (i.e., critical diameter) was found to increase from 136 nm to 220 nm after carbonation curing. The critical diameter represents the largest interconnected pores that control the transport behavior in cementitious materials. Thus, the increased critical diameter indicates a possible raise in water permeation of the carbonated ECC. Table 9 breaks down the porosity and pore volume fraction in three different pore size intervals, i.e., >100 nm, 10–100 nm, and <10 nm. The porosity above 100 nm was found to be the same (i.e., 12.7%) between carbonation curing and non-carbonated reference. However, the latter exhibited higher porosity and pore volume fraction for pores smaller than 10 nm (i.e., small capillary and gel pores) [38]. The increase of pores in this category can be associated with the products of pozzolanic reaction and account for the lowered average pore size in the non-carbonated ECC.

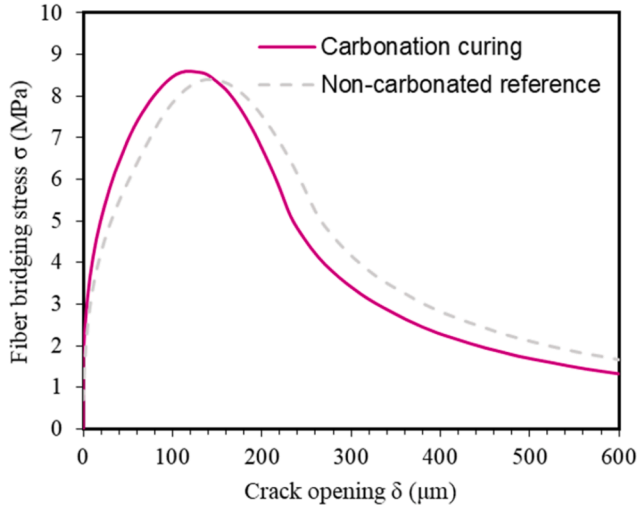

Fig. 13. Fiber bridging curves predicted for Mix I at 28 days.

When loaded in tension, ECC's crack control ability was amplified by carbonation curing, exhibiting tighter cracks and more saturated multiple cracking. The effect of carbonation curing on ECC crack width distribution is shown in Fig. 15, and the average crack widths are summarized in Table 10. Carbonation curing was found to reduce the average crack width in ECC at all strain levels. The maximum crack width and average crack spacing were also decreased, indicating more distinct characteristics of multiple fine cracking after carbonation curing. The reduction in crack width can be related to the more robust fiber bridging behavior and the denser fiber/matrix interface induced by carbonation curing.

Results from the permeability test suggest that carbonation curing may accelerate the water permeation in uncracked ECC but would decrease ECC's permeability in cracked condition. As can be seen in Fig. 16, the coefficient of permeability k in the uncracked ECC increased from 1.3×10^{-11} m/s to 2.6×10^{-11} m/s after carbonation curing. This agrees with the increased pore size and capillary pore volume in the carbonated ECC despite a smaller total porosity. As indicated in Table 9, the reduction of total porosity after carbonation curing stems from the lowered volume of small capillary and gel pores that play a relatively minor role in water permeation [38]. As such, although the matrix can be densified by $CaCO_3$ precipitation, the pore refinement effect associated with pozzolanic reaction is compromised, leading to an increased percentage of water permeable pores after carbonation curing.

In loaded condition, the crack width becomes the dominating factor that governs the material permeability [12,20]. As shown in Fig. 16, the coefficient of permeability was lowered by carbonation curing at all strain levels. This agrees with the reduction of crack width as discussed above. The coefficient of permeability appeared to increase with the imposed tensile strain and was found in the ranges of 5.33×10^{-11}–1.70×10^{-9} m/s for the carbonated ECC and 1.50×10^{-10}–2.10×10^{-9} m/s for the non-carbonated ECC on an average basis. It indicates that the more robust crack control capability led by carbonation curing overshadows the negative impact of the increased pore size on water permeability. It is worth mentioning that upon the completion of the water permeability test fewer cracks were found to be filled with white residues in the carbonated specimens compared to the non-carbonated reference, suggesting that the self-healing process may be lowered or slowed down after carbonation curing. In this study, the coefficient of water permeability stabilized at 20 days and was thus terminated for comparison. Further investigations may address its long-term evolution beyond this age and clarify the extent of self-healing in diverse environments, such as wet-dry cycles and salt solutions.

4. Conclusions

The present study develops a carbonation curing process for Engineered Cementitious Composites (ECC) containing PVA fiber and high-volume fly ash and examines the impacts of carbonation on the composite mechanical and transport properties. The key findings are as follows.

- Lab-scale ECC specimens (13-mm specimen thickness) achieve a 29.6–35.1% CO_2 uptake by cement mass and a fully carbonated cross section after 24 h of early carbonation. The high fly ash content is responsible for ECC's significant carbonation efficiency. In turn, carbonation curing mostly depletes the fly ash pozzolanic reaction by lowering the binder alkalinity. The absence of pozzolanic reaction may hinder the long-term binding ability and create a potentially larger pore size compared to the non-carbonated reference. Therefore, for ultrahigh volume fly ash ECC (fly ash-to-cement mass ratio > 2.2), the trade-off between CO_2 uptake and pozzolanic reaction should be considered.

Table 7
Strain-hardening indices for Mix I at 28 days.

Curing condition	Energy criterion			Strength criterion		
	J_b' (J/m^2)	J_{tip} (J/m^2)	PSH_{energy}	σ_0 (MPa)	σ_{fc} (MPa)	$PSH_{strength}$
Carbonation curing	208 ± 47.5	7.12 ± 1.31	29.2 ± 12.0	8.59 ± 0.41	5.30 ± 0.37	1.62 ± 0.19
Non-carbonated reference	280 ± 34.1	8.44 ± 1.42	33.2 ± 9.62	8.40 ± 0.22	4.21 ± 0.03	2.00 ± 0.07

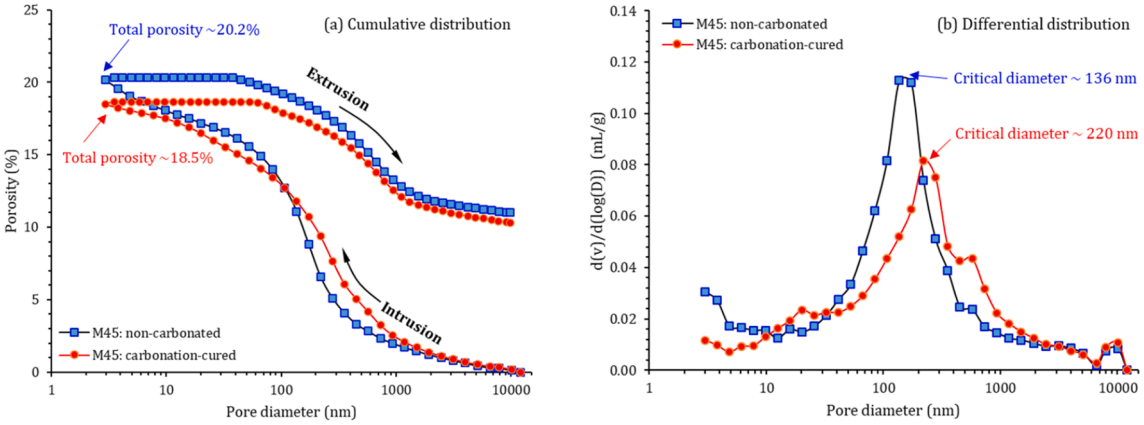

Fig. 14. MIP pore size distribution for Mix I at 28 days.

Table 8
ECC pore structure properties for Mix I at 28 days.

Pore structure parameter	Carbonation curing	Non-carbonated reference
Total intruded volume, mL/g	0.091	0.105
Total porosity, %	18.5	20.2
Median pore diameter, nm	224	152
Average pore diameter, nm	47	31
BET Surface area, m^2/g	7.821	13.579

Table 9
ECC porosity and pore volume fraction breakdown for Mix I at 28 days.

Curing condition	Pore size range	Porosity, %	Fraction of total pore volume, %
Carbonation curing	>100 nm	12.7	68.7
	10–100 nm	5.3	28.9
	<10 nm	0.4	2.4
Non-carbonated reference	>100 nm	12.7	62.6
	10–100 nm	4.9	24.2
	<10 nm	2.6	12.8

- In the ECC with a fly ash-to-cement mass ratio of 1.2, carbonation curing enhances material mechanical properties immediately after carbonation and at standard 28 days. At 2 days, ECC's ultimate tensile and compressive strengths were accelerated by 57.2% and 40.9%, respectively, due to the accelerated cement reaction driven by the early-age carbonation. At 28 days, the matrix and fiber/matrix interface were found densified leading to a composite ultimate tensile strength of 7.94 MPa (6.47 MPa for non-carbonated reference). The 28-day tensile strain capacities were found to be comparable between carbonation curing and the non-carbonated reference (i.e., 4.42% versus 4.77%).
- At the fiber/matrix interface, carbonation curing improves the chemical and frictional bonds leading to a robust crack width control. The tighter crack width reduces ECC's water permeability in loaded condition, despite a more permeable matrix due to a larger pore size associated with the lowered pozzolanic reaction. As field structures are mostly in stress and prone to cracking, the enhanced

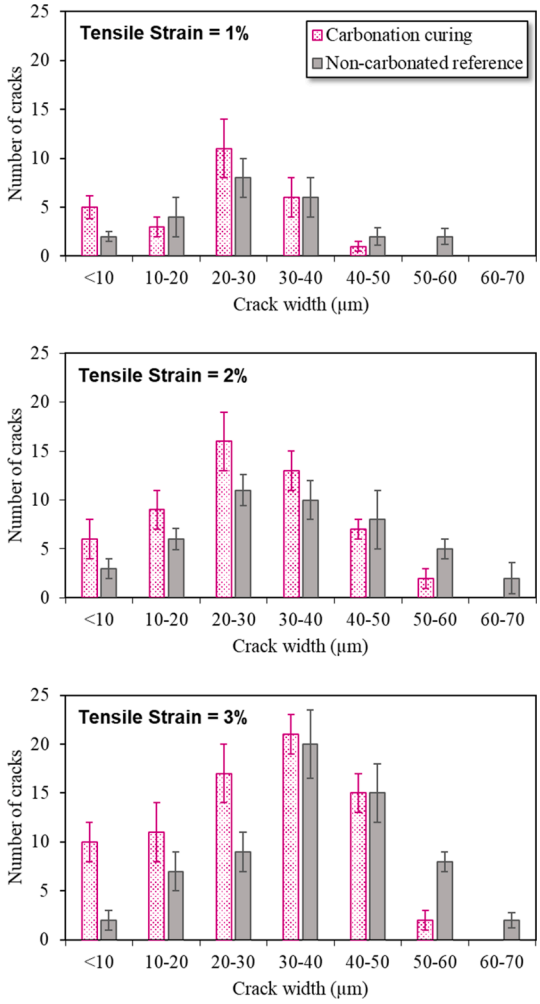

Fig. 15. Crack width distribution in loaded condition for Mix I at 28 days.

Table 10
ECC average crack width and spacing in loaded condition for Mix I at 28 days.

Tensile strain	Average crack width (μm)		Average crack spacing (mm)	
	Carbonation curing	Non-carbonated reference	Carbonation curing	Non-carbonated reference
1%	22 ± 6	33 ± 3	2.9 ± 0.3	3.8 ± 0.6
2%	26 ± 9	38 ± 8	1.5 ± 0.3	2.1 ± 0.2
3%	27 ± 9	41 ± 15	1.1 ± 0.2	1.7 ± 0.1

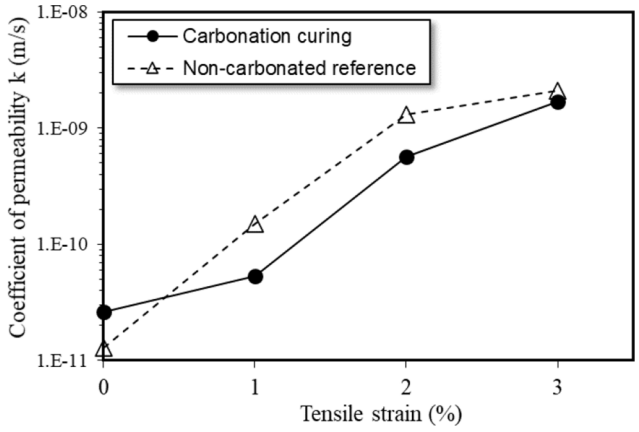

Fig. 16. Coefficient of water permeability in non-loaded and loaded conditions for Mix I; Tests began at 28 days and lasted for 20 days.

crack width control and lowered water permeability by carbonation curing are expected to improve the durability of structures made with ECC.

This study establishes the viability of applying carbonation curing to ECC, with technical merits of accelerated early strength/ductility, tighter crack width, and lowered permeability to water-borne harmful species in loaded condition. Beyond the remarkable CO_2 sequestration capacity at the manufacturing stage, ECC after carbonation curing is anticipated to lower the lifecycle emissions as an example of beneficially utilizing CO_2 for durable precast construction products. Further investigations on lifecycle and techno-economic assessments may assist with the process optimization and accelerate industrial implementations at scale.

CRediT authorship contribution statement

Duo Zhang: Data curation, Formal analysis, Investigation, Validation, Writing – original draft. **Brian R. Ellis:** Funding acquisition, Project administration, Writing – review & editing. **Beata Jaworska:** Data curation, Formal analysis, Investigation, Validation. **Wei-Hsiu Hu:** Investigation, Validation. **Victor C. Li:** Conceptualization, Funding acquisition, Project administration, Resources, Writing – review & editing.

Declaration of Competing Interest

The authors declare that they have no known competing financial interests or personal relationships that could have appeared to influence the work reported in this paper.

Acknowledgment

Financial support for this work was provided by the U.S. Department of Energy, National Energy Technology Laboratory (NETL) through award No. DE-FE0030684.

References

[1] D. Zhang, Z. Ghouleh, Y. Shao, Review on carbonation curing of cement-based materials, J. CO2 Util. 21 (2017) 119–131.
[2] D. Zhang, V.C. Li, B.R. Ellis, Optimal pre-hydration age for CO2 sequestration through Portland cement carbonation, ACS Sustainable Chem. Eng. 6 (12) (2018) 15976–15981.
[3] V. Rostami, et al., Microstructure of cement paste subject to early carbonation curing, Cem. Concr. Res. 42 (1) (2012) 186–193.
[4] D. Zhang, X. Cai, B. Jaworska, Effect of pre-carbonation hydration on long-term hydration of carbonation-cured cement-based materials, Constr. Build. Mater. 231 (2020), 117122.
[5] D. Zhang, Y. Shao, Surface scaling of CO2-cured concrete exposed to freeze-thaw cycles, J. CO2 Util. 27 (2018) 137–144.
[6] D. Zhang, T. Liu, Y. Shao, Weathering carbonation behavior of concrete subject to early-age carbonation curing, J. Mater. Civ. Eng. 32 (4) (2020) 04020038.
[7] V. Rostami, Y. Shao, A.J. Boyd, Durability of concrete pipes subjected to combined steam and carbonation curing, Constr. Build. Mater. 25 (8) (2011) 3345–3355.
[8] D. Zhang, Y. Shao, Enhancing chloride corrosion resistance of precast reinforced concrete by carbonation curing, ACI Mater. J. 116 (3) (2019) 3–12.
[9] D. Zhang, B. Jaworska, Effect of carbonation curing on Portland cement MgSO 4 attack: laboratory characterization at 900 days, J. Mater. Civ. Eng. 33 (4) (2021) 04021032.
[10] D. Zhang, V.C. Li, B.R. Ellis, Ettringite-related dimensional stability of CO2-cured Portland cement mortars, ACS Sustainable Chem. Eng. 7 (19) (2019) 16310–16319.
[11] H. El-Hassan, Y. Shao, Z. Ghouleh, Effect of Initial Curing on Carbonation of Lightweight Concrete Masonry Units, ACI Mater. J. 110 (4) (2013) 441–450.
[12] H. Liu, et al., Influence of micro-cracking on the permeability of engineered cementitious composites, Cem. Concr. Compos. 72 (2016) 104–113.
[13] V.C. Li, Engineered Cementitious Composites (ECC): Bendable Concrete for Sustainable and Resilient Infrastructure. 2019: Springer.
[14] V.C. Li, On engineered cementitious composites (ECC). A review of the material and its applications, J. Adv. Concr. Technol. 1 (3) (2003) 215–230.
[15] V.C. Li, From micromechanics to structural engineering-the design of cementitous composites for civil engineering applications. 1993.
[16] V.C. Li, S. Wang, C. Wu, Tensile strain-hardening behavior of polyvinyl alcohol engineered cementitious composite (PVA-ECC), ACI Mater. J.-Am. Concr. Inst. 98 (6) (2001) 483–492.
[17] V.C. Li, Engineered cementitious composites (ECC) - tailored composites through micromechanical modeling, in: N. Banthia, A. Bentur, A.A. Mufti (Eds.), Fiber Reinforced Concrete Present and Future, Canadian Society for Civil Engineering, Montreal (Canada), 1997, pp. 64–97.
[18] V.C. Li, et al., Interface tailoring for strain-hardening Polyvinyl Alcohol-Engineered Cementitious Composite (PVA-ECC), ACI Mater. J. 99 (5) (2002) 463–472.
[19] V.C. Li, Engineered cementitious composites (ECC) material, structural, and durability performance. Concrete Construction Engineering Handbook, ed. N. E. 2008: CRC Press.
[20] M.D. Lepech, V.C. Li, Water permeability of engineered cementitious composites, Cem. Concr. Compos. 31 (10) (2009) 744–753.
[21] E.N. Herbert, V.C. Li, Self-healing of microcracks in Engineered Cementitious Composites (ECC) under a natural environment, Materials 6 (7) (2013) 2831–2845.
[22] Y. Yang, et al., Autogenous healing of engineered cementitious composites under wet–dry cycles, Cem. Concr. Res. 39 (5) (2009) 382–390.
[23] D. Zhang, et al., Autogenous healing of Engineered Cementitious Composites (ECC) based on MgO-fly ash binary system activated by carbonation curing, Constr. Build. Mater. 238 (2020), 117672.
[24] S. Wang, V.C. Li, Engineered cementitious composites with high-volume fly ash, ACI Mater. J. 104 (3) (2007) 233.
[25] D. Zhang, Y. Shao, Early age carbonation curing for precast reinforced concretes, Constr. Build. Mater. 113 (2016) 134–143.
[26] D. Zhang, X. Cai, Y. Shao, Carbonation curing of precast fly ash concrete, J. Mater. Civ. Eng. 28 (11) (2016) 04016127, https://doi.org/10.1061/(ASCE)MT.1943-5533.0001649.
[27] H. El-Hassan, Y. Shao, Early carbonation curing of concrete masonry units with Portland limestone cement, Cem. Concr. Compos. 62 (2015) 168–177.
[28] K. Scrivener, R. Snellings, B. Lothenbach, A Practical Guide to Microstructural Analysis of Cementitious Materials. 2016: Crc Press.
[29] D. Zhang, Y. Shao, Effect of early carbonation curing on chloride penetration and weathering carbonation in concrete, Constr. Build. Mater. 123 (2016) 516–526.
[30] JSCE, Recommendations for Design and Construction of High Performance Fiber Reinforced Cement Composites with Multiple Fine Cracks (HPFRCC). 2008: Tokyo.
[31] E.-H. Yang, Y. Yang, V.C. Li, Use of high volumes of fly ash to improve ECC mechanical properties and material greenness, ACI Mater. J. 104 (6) (2007) 620.
[32] Y.A. Villagrán-Zaccardi, et al., Recommendation of RILEM TC 238-SCM: determination of the degree of reaction of siliceous fly ash and slag in hydrated cement paste by the selective dissolution method, Mater. Struct. 51 (1) (2018) 27.
[33] C. Redon, et al., Measuring and modifying interface properties of PVA fibers in ECC matrix, J. Mater. Civ. Eng. 13 (6) (2001) 399–406.
[34] E.-H. Yang, et al., Fiber-bridging constitutive law of engineered cementitious composites, J. Adv. Concr. Technol. 6 (1) (2008) 181–193.
[35] Y. Shao, et al., Accelerated carbonation of portland limestone cement, J. Mater. Civ. Eng. 26 (1) (2014) 117–124.

[36] D. Ravikumar, et al., Carbon dioxide utilization in concrete curing or mixing might not produce a net climate benefit, Nat. Commun. 12 (1) (2021) 1–13.
[37] C.-F. Chang, J.-W. Chen, Strength and elastic modulus of carbonated concrete, Mater. J. 102 (5) (2005) 315–321.
[38] K.K. Aligizaki, Pore structure of Cement-based Materials: Testing, Interpretation and Requirements. 2014: CRC Press.